RESEARCH ARTICLE | MARCH 23 2023

High open-circuit voltage in single-crystalline n-type SnS/MoO$_3$ photovoltaics ⊕

Issei Suzuki ✉ ⓘ ; Zexin Lin; Taichi Nogami; Sakiko Kawanishi ⓘ ; Binxiang Huang ⓘ ; Andreas Klein ⓘ ;
Takahisa Omata ⓘ

Check for updates

CrossMark

View Online   Export Citation

High open-circuit voltage in single-crystalline n-type SnS/MoO₃ photovoltaics EP

View Online   Export Citation   CrossMark

Issei Suzuki,[1,a] ID Zexin Lin,[1] Taichi Nogami,[1] Sakiko Kawanishi,[1] ID Binxiang Huang,[2] ID Andreas Klein,[2] ID
and Takahisa Omata[1] ID

AFFILIATIONS

[1] Institute of Multidisciplinary Research for Advanced Materials (IMRAM), Tohoku University, 2-1-1 Katahira, Aoba-ku,
Sendai 980-8577, Japan

[2] Department of Materials and Earth Science, Electronic Structure of Materials, Technical University of Darmstadt,
Otto-Berndt-Str. 3, 64287 Darmstadt, Germany

[a] Author to whom correspondence should be addressed: issei.suzuki@tohoku.ac.jp

ABSTRACT

It has been recently reported that n-type single crystalline SnS exhibits a large band bending (~1 eV) at the interface with MoO₃, which is a large work function material. In this study, we applied this interface to solar cells for the first time and evaluated its photovoltaic properties. The highest V_{OC} achieved was 437 mV. Although this value is the highest ever recorded for SnS solar cells, it was lower than the expected value of 700–800 mV. The highest power conversion efficiency (PCE) was 4.4%. Based on an analysis of the device parameters, we propose methods for improving the device performance, including V_{OC}, the short-circuit current, and PCE. The carrier-collection length of the n-type SnS single crystals was estimated to be ~200 nm based on the external quantum efficiency measurements. Therefore, this study demonstrates that the V_{OC} of SnS solar cells can be improved by fabricating a junction with MoO₃ thin films.

I. INTRODUCTION

Semiconductors consisting of safe and abundant elements are required as thin-film solar cell materials to supersede CdTe or Cu(In,Ga) (S,Se), which contain toxic or rare elements.[1] Sulfides such as Cu_2ZnSnS_4,[2] Cu_2SnS_3,[3] and Sb_2S_3[4] have attracted much attention because of their suitable optical properties for photovoltaic application, among which SnS has been actively studied due to its simple binary system and synthetic ease.[5–7] Because undoped SnS generally exhibits p-type electrical conduction, heterojunction thin-film solar cells containing p-type SnS and other n-type semiconductors, such as CdS and Zn(O,S), have been studied for more than two decades. However, their open-circuit voltage (V_{OC}) is low[8] at 300–400 mV and results in a maximum power conversion efficiency (PCE) of only 4.8%.[9]

It was recently reported that single-crystalline SnS exhibits significant band bending at the interface with MoO₃.[10] The observed band bending (~1 eV) is almost equal to the bandgap of SnS. This indicates that there is no fundamental limitation to the photovoltage that can be generated by SnS solar cells, in contrast to the case for

cells based on other photovoltaic semiconductors, such as CuGaSe₂, whose V_{OC} is limited by the Fermi level pinning mechanism.[11] Thus, SnS is a promising photovoltaic material, based on its potential V_{OC}. Moreover, SnS/MoO₃ junctions should find wide applicability in solar cells. In these junctions, as shown in Fig. 1, the photogenerated electrons and holes within SnS move to the left and right, respectively, resulting in significant band bending (~1 eV) and a V_{OC} of 700–800 mV.[12]

In this study, solar cells based on junctions of n-type SnS single crystals and MoO₃ thin films with different conductivities were fabricated, and their performances were analyzed. In addition, a strategy for achieving a PCE of more than 10% in these devices by improving V_{OC} and the short-circuit current (J_{SC}) was evaluated and is proposed herein.

II. EXPERIMENTAL

SnS single crystals: Br-doped n-type single-crystalline SnS (orthorhombic α-SnS) was prepared using a previously reported
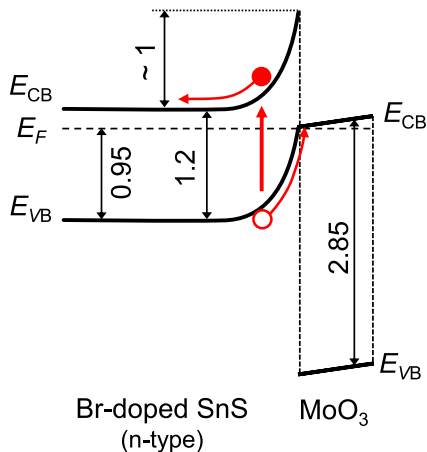
FIG. 1. Schematic of the band structure at the interface between n-type SnS and MoO$_3$ based on a previous photoelectron spectroscopy study.[10] The arrows indicate electron/hole transport. E_{CB}, E_{VB}, and E_F represent the energies of the conduction band minimum, valence band maximum, and Fermi level, respectively. Values are in eV.
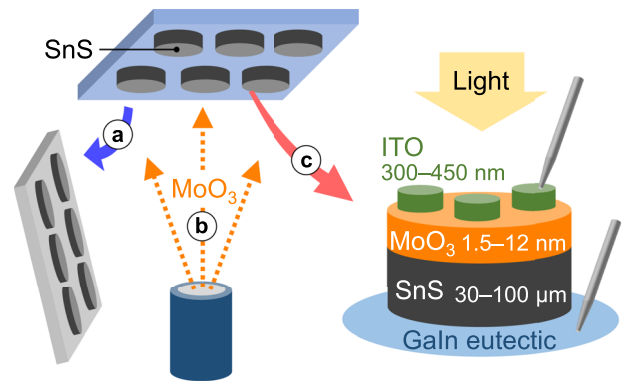

FIG. 2. Schematic of the procedure for fabricating the ITO/MoO$_3$/SnS device, which included the following three steps: (a) cleavage of n-type SnS single crystals, (b) deposition of a MoO$_3$ thin film, and (c) fabrication of front and back electrodes.

flux method.[13] The Br concentration, carrier electron concentration, and Hall mobility of the single crystals used in this study were ~0.30 at. % (corresponding to ~6 × 10^{19} cm^{-3}), ~6 × 10^{17} cm^{-3}, and ~150 cm^2 V^{-1} s^{-1}, respectively. These values are comparable to those reported in the previous study.

Device fabrication: The fabrication of the solar cells involved three steps, as illustrated in Fig. 2. First, a SnS single crystal with a thickness of 30–100 μm was cut into a circle with a diameter of 3–5 mm, and 6–8 such crystal pieces were fixed to the sample holder (blue plate in Fig. 2) using adhesive Ag paste (Muromach bond H220, Muromachi Chemicals Inc., Japan). Next, a metal plate (gray plate in Fig. 2) was fixed to the surfaces of the single crystals using epoxy glue (Toll Seal, Agilent Technologies, CA, USA) and then removed in a deposition vacuum chamber (pressure lower than 9 × 10^{-6} Pa) to cleave off single crystals. Second, the MoO$_3$ layer was deposited onto the clean surfaces of the cleaved SnS single crystals via resistive thermal evaporation (CH140, The Nilaco Corporation, Japan). The distance between the SnS crystals and the evaporation source was ~12 cm. To determine the deposition rate and electrical conductivity of the MoO$_3$ layer, a thick MoO$_3$ film (several hundred nanometers in thickness) was deposited onto a SiO$_2$ glass substrate and subjected to thickness and electrical measurements. MoO$_3$ layers with different electrical conductivities were used in this study: (i) low-conductivity MoO$_3$ layers—MoO$_3$ powder (99.999%, Strem Chem., MA, USA) was used as the source, and evaporation was performed at 550 °C, resulting in a deposition rate of ~4.0 nm min^{-1} and an electronic conductivity (σ_{MoO_3}) of 1.7 × 10^{-8} S cm^{-1}—and (ii) high-conductivity MoO$_3$ layers, for which the as-purchased MoO$_3$ powder was annealed at 500 °C for 5 h in vacuum (~5 × 10^{-5} Pa) to enhance the electrical conductivity of MoO$_3$ (σ_{MoO_3}),[14] followed by evaporation at 500 °C; this procedure resulted in a deposition rate of ~0.15 nm min^{-1} and σ_{MoO_3} of 2.4 × 10^{-5} S cm^{-1}. X-ray photoelectron spectroscopy showed that the vacuum annealing of the source powder resulted in MoO$_3$ films with a higher Mo^{5+} content, indicating that oxygen vacancies were incorporated within the films, which

increased their carrier concentration (Fig. S1 in the supplementary material).[15] Notably, while the introduction of oxygen vacancies in MoO$_3$ reduced its work function slightly (~6.9 and ~6.6 eV for MoO$_3$ and MoO$_{2.9}$, respectively),[16] it remained significantly larger than that of SnS (4.2 eV)[10] without affecting the band-bending width of SnS. Finally, a SnO$_2$-doped In$_2$O$_3$ (ITO) layer was deposited onto the MoO$_3$ film as a transparent top electrode via radio frequency (RF) magnetron sputtering (KSP-120-LLGB, Kenix, Japan) using a metallic mask with holes. A 1-in.-diameter ITO compact (SnO$_2$ 10 wt. %–In$_2$O$_3$, Mitsui Mining and Smelting Co., Ltd., Japan) was used as the sputtering target. Deposition was performed without intentional heating at 0.9 Pa and an RF power of 20 W in a flow of Ar (10 SCCM). The area, thickness, and sheet resistance of the ITO layer were 0.4–0.6 mm^2, ~300 nm, and ~20 Ω $\square^{-1}$, respectively. A Ga–In eutectic (99.999%, Ga 75.5 wt. %–In 24.5 wt. %, Kojundo Chemical Laboratory Co., Ltd., Japan) was coated onto the bottom of the SnS single crystals as the back electrode.

Characterization: The J–V characteristics of the fabricated solar cells were measured using a direct current (DC) voltage current source/monitor (TR6143, Advantest Corporation, Japan). A 150-W Xe lamp (SM-30, Bunkoukeiki Co., Ltd., Japan) with a total reflection mirror and an AM1.5 filter was used as the light source. The irradiance was calibrated to 1 sun using a silicon photodiode (BS-500BK, Bunkoukeiki Co., Ltd., Japan). The device parameters, such as the series resistance (R_s), shunt resistance (R_{sh}), reverse saturation current (J_0), and ideality factor of the diode (n), were obtained by fitting the J–V curve using the following equation:

$$J = J_{ph} - J_0\{\exp[q(V + JR_s)/nk_BT] - 1\} - (V + JR_s)/R_{sh}, \quad (1)$$

where J_{ph}, k_B, T, and q are the photogenerated current density, Boltzmann constant, temperature, and elementary charge, respectively. The initial values of each parameter prior to fitting were obtained from a numerical analysis of the J–V curve, as reported by Hegedus and Shafarman.[17]

The external quantum efficiency (EQE) spectra of the fabricated solar cells were measured using a monochromatic light source (SM-30, Bunkoukeiki Co., Ltd., Japan). The spectral irradiance was calibrated using a Si photodiode (S1337-1010BQ, Bunkoukeiki

Co., Ltd., Japan). The EQE of the ITO/MoO$_3$/SnS device was also simulated using the e-ARC code.[18,19] The experimentally determined optical properties of the ITO,[20] MoO$_x$,[18] and SnS thin films (absorption coefficient[21] and refractive index[22]) were used for the calculations.

III. RESULTS

Figure 3 shows the typical $J–V$ curves for the devices fabricated using MoO$_3$ layers with thicknesses of 3 and 6 nm. A photocurrent was generated when the devices were irradiated with light, confirming that the n-type SnS/MoO$_3$ junctions are suitable for use in solar cells. The photovoltaic properties of the device with the highest PCE for each MoO$_3$ layer thickness are listed in Table I. The photovoltaic properties of the devices based on the low-conductivity MoO$_3$ layers with thicknesses of 1.5 and 12 nm are described in Note 1 in the supplementary material. Briefly, the V_{OC} values of the devices with the 1.5 and 12 nm-thick MoO$_3$ thin films were lower than those of the devices based on the films with the optimal thickness, which was ~3–6 nm.

The highest V_{OC} (437 mV) was achieved in the case of the device with a 6-nm-thick low-conductivity MoO$_3$ layer, whereas the highest PCE (4.2%) was obtained in the case of the device with the 3-nm-thick high-conductivity MoO$_3$ layer. The highest and second highest previously reported V_{OC} values for SnS heterojunction solar cells were 405 and 400 mV, respectively.[23,24] Therefore, the record V_{OC} achieved in this study indicate that the n-type SnS single crystal/MoO$_3$ junction is appropriate for ensuring a high V_{OC}. However, the expected V_{OC} (700–800 mV) was not obtained, and there is room for further improvements. In Sec. IV, we discuss the reason for

the obtained V_{OC} being lower than the expected value and propose a strategy for improving it.

Figure 4 shows the relationship between the conductivity and thickness of the MoO$_3$ layer as well as the photovoltaic properties and device parameters of the fabricated solar cells. V_{OC} and J_{SC} were almost independent of the film thickness and conductivity [Figs. 4(a) and 4(b)]. By contrast, the fill factor (FF) increased with increasing MoO$_3$ conductivity, and accordingly, PCE showed a minor positive trend. Because a large R_s lowers FF, the increase in FF is ascribed to the decrease in R_s. Because the resistance of the semi-insulating MoO$_3$ layer contributes considerably to R_s, it is reasonable that R_s was reduced owing to the enhanced conductivity of MoO$_3$.

Figure 5 shows the EQE spectrum of the device with a 6-nm-thick high-conductivity MoO$_3$ layer. The devices with the MoO$_3$ thin films of different conductivities and thicknesses had almost identical EQE spectra (Fig. S4). This is consistent with the fact that J_{SC} is independent of the conductivity and thickness of MoO$_3$ [Fig. 4(b)]. The EQE is typically 80%–90% in the wavelength range of 350–600 nm. The sharp decrease in EQE observed in the short-wavelength region (~350 nm) is due to the fundamental absorption of the ITO layer.[25] Moreover, a gradual decrease in EQE was observed in the long-wavelength region (600–1000 nm). The bandgap determined from the absorption edge (~970 nm) was ~1.3 eV (Fig. S3), which corresponded to the direct bandgap of SnS.[13] Such a gradual decrease in EQE is typical of devices composed of light-absorbing layers with short carrier-collection lengths (L_c).[19,25] L_c is defined by the following equation:
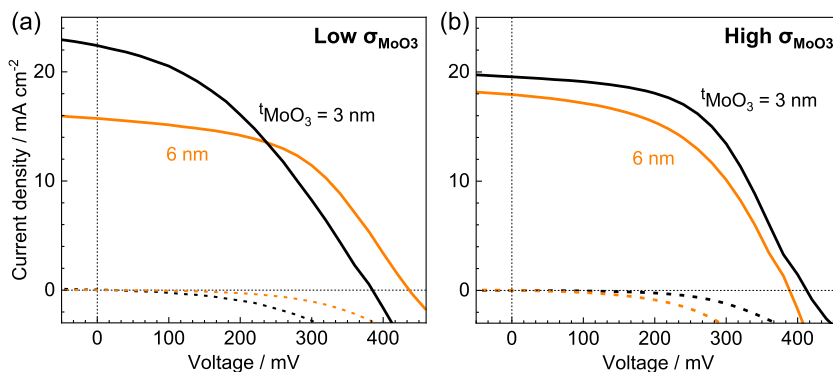
$$L_c = W + L_{diff}, \qquad (2)$$

FIG. 3. $J–V$ characteristics of representative solar cells fabricated using n-type SnS single crystal/MoO$_3$ junctions with MoO$_3$ layers of different thicknesses and (a) low and (b) high conductivities as determined under illumination (solid lines) and in the dark (dashed lines).

TABLE I. Photovoltaic characteristics of the representative solar cells fabricated using n-type SnS single crystal/MoO$_3$ junctions with MoO$_3$ layers of different thicknesses and conductivities.

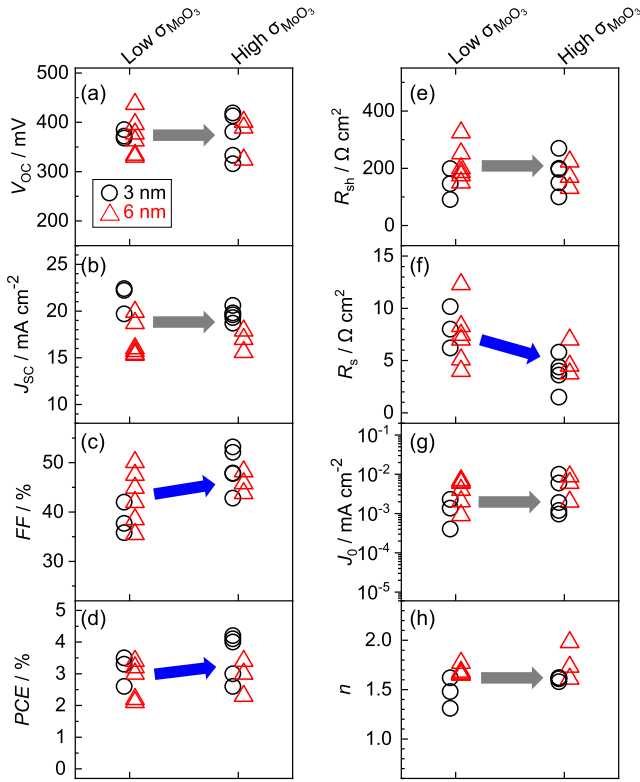| MoO$_3$ layer conductivity	MoO$_3$ layer thickness (nm)	PCE (%)	V_{OC} (mV)	J_{SC} (mA cm^{-2})	FF (%)	R_{sh} (Ω cm^2)	R_s (Ω cm^2)	J_0 (mA cm^{-2})	n
Low σ_{MoO_3}	3	3.3	385	22.4	37.7	146	8.0	2.3×10^{-3}	1.48
(1.7×10^{-8} S cm^{-1})	6	3.4	437	15.7	50.1	200	7.5	9.0×10^{-4}	1.77
High σ_{MoO_3}	3	4.2	413	19.6	52.1	270	3.6	1.2×10^{-3}	1.62
(2.4×10^{-5} S cm^{-1})	6	3.4	389	17.9	48.2	223	3.8	8.7×10^{-3}	1.98

FIG. 4. Photovoltaic properties and device parameters of n-type SnS single crystal/MoO₃ junctions with MoO₃ layers of different thicknesses (3 and 6 nm) and conductivities: (a) V_{OC}, (b) J_{SC}, (c) FF, (d) PCE, (e) R_{sh}, (f) R_s, (g) J_0, and (h) n. Arrows indicate change direction with increase in MoO₃ conductivity.

where W and L_{diff} are the width of the space-charge region and diffusion length of the minority carriers, respectively.[19]

The EQE of the junction of the ITO/MoO₃/n-type SnS single-crystal was simulated for different L_c values using the e-ARC
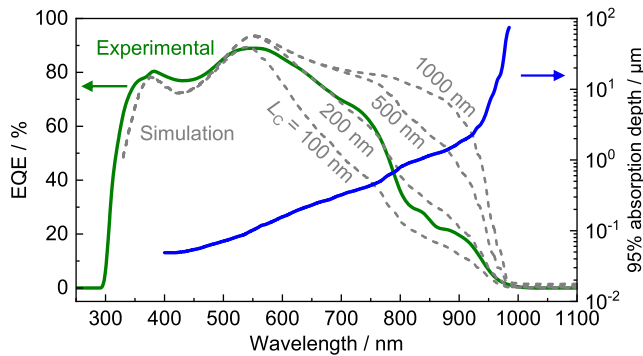

FIG. 5. EQE spectra of solar cells with n-type SnS single crystal/MoO₃ film junctions with a 6-nm-thick high-conductivity MoO₃ layer. Gray lines represent EQE spectra simulated using e-ARC for different L_c values. The blue line represents the depth at which 95% of light is absorbed based on the absorption coefficient of SnS.[21]

code.[18,19] For L_c = 200 nm, the measured and simulated EQE spectra agreed well, as shown in Fig. 5. Therefore, L_c in the n-type SnS single crystal should be ~200 nm. Because the effective donor density of the n-type SnS single crystal is large, the W value of the n-type SnS single crystal at the interface with MoO₃ is small (~10 nm)[5] and considerably lower than L_c (i.e., W ≪ L_c), indicating that L_{diff} is comparable to L_c (i.e., $L_{diff} ≈ L_c ≈$ 200 nm).

IV. DISCUSSION

The highest V_{OC} achieved was 437 mV, which is considerably smaller than the expected value (700–800 mV), as derived from the extent of band bending (~1 eV). V_{OC} was obtained by setting J = 0 in Eq. (1). Assuming that $J_{ph} = J_{SC}$ owing to R_s is sufficiently small, $J_0 ≪ J_{SC}$ and $V_{OC}/J_{SC} ≪ R_{sh}$. Thus, V_{OC} can be calculated using the following equation:

$$V_{OC} = \frac{nk_BT}{q}\ln\left(\frac{J_{SC}}{J_0}\right). \quad (3)$$

The J_0 values of the fabricated devices were of the order of 10^{-3} mA cm^{-2} [Fig. 4(g)], which is 2–3 orders of magnitude higher than those of devices exhibiting good V_{OC}. For example, $J_0 = ~4 \times 10^{-6}$ mA cm^{-2} for Cu(InGa)(SSe)₂ cells (V_{OC} = 623 mV) and ~7 × 10^{-5} mA cm^{-2} for Cu₂ZnSnSe₄ cells (V_{OC} = 513 mV).[26] To estimate the increase in V_{OC} with decreasing J_0, the J–V curve was simulated using a reduced J_0 (10^{-5} mA cm^{-2}) and the parameter values for the device with a PCE of 4.2%. This resulted in an increased V_{OC} of 600 mV [Fig. 6(b)]. Therefore, reducing J_0 is the most promising strategy for increasing V_{OC}.

J_0 is determined by the recombination current around the space-charge region when $n ≈ 2$. The single crystal contains a high
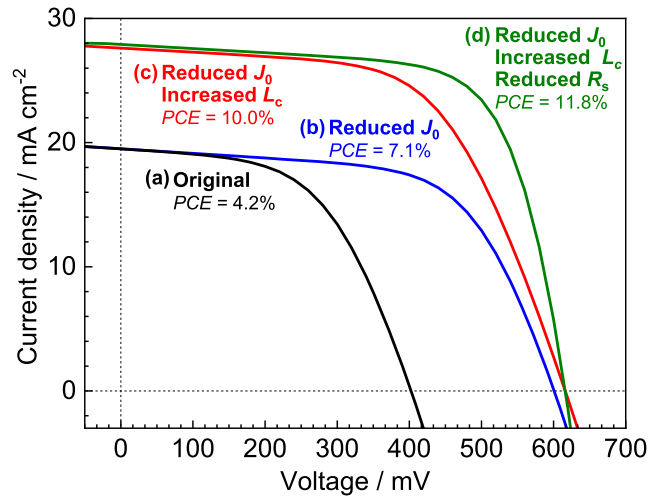

FIG. 6. Simulated J–V curves with experimentally determined and modified device parameters (R_s, J_0, and L_c). (a) J–V curve with experimentally determined device parameters for the cell with the highest PCE (R_s = 4.2 Ω cm², R_{sh} = 300 Ω cm², $J_0 = 1.0 \times 10^{-3}$ mA cm^{-2}, and L_c = 200 nm). J–V curve with (b) reduced J_0 (1.0 × 10^{-5} mA cm^{-2}), (c) reduced J_0 and increased L_c (1000 nm), and (d) reduced J_0, increased L_c, and reduced R_s (1.0 Ω cm²). Specific input and output values are listed in Table II. R_{sh} = 300 Ω cm².

TABLE II. Device parameters used for simulation (left) and output photovoltaic characteristics (right) corresponding to the J–V curves shown in Fig. 6.

	Input parameters			Output parameters			
	R_s (Ω cm^2)	J_0 (mA cm^{-2})	L_c (nm)	V_{OC} (mV)	J_{SC} (mA cm^{-2})	FF (%)	PCE (%)
(a) Original	4.2	1.0×10^{-3}	200	401	20	54	4.2
(b) Reduced J_0	4.2	1.0×10^{-5}	200	600	20	61	7.1
(c) Reduced J_0 and increased L_c	4.2	1.0×10^{-5}	1000	616	28	59	10.0
(d) Reduced J_0, increased L_c, and reduced R_s	1	1.0×10^{-5}	1000	615	28	69	11.8

concentration of the dopant ($\sim 6 \times 10^{19}$ cm^{-3}), which is two orders of magnitude higher than the carrier concentration. This means that the dopant mostly remains inactivated and does not generate carrier electrons. The effective donor concentration estimated from capacitance–voltage measurements was also considerably higher than the carrier concentration,[5] indicating the existence of deep defect levels. As is also the case for Cu$_2$ZnSnS$_4$ solar cells, whose V_{OC} increases with a decrease in the concentration of the deep acceptor Cu$_{Zn}$,[27] decreasing the dopant concentration in the n-type SnS single crystal is the most straightforward approach for reducing J_0 and, hence, increasing V_{OC}.

J_{SC} is determined by L_{diff}, which is given by the following equation:[28]

$$L_{diff} = \sqrt{D\tau}, \qquad (4)$$

where D and τ are the minority-carrier diffusion coefficient and lifetime, respectively. τ is defined as the harmonic sum of the lifetimes corresponding to the various recombination mechanisms of the minority carriers, as given by[28]

$$\frac{1}{\tau} = \frac{1}{\tau_{rad}} + \frac{1}{\tau_{Auger}} + \frac{1}{\tau_{SRH}} + \frac{1}{\tau_{surface}} \cdots, \qquad (5)$$

where τ_{rad} and τ_{Auger} represent the radiative and Auger lifetimes, respectively, and τ_{SRH} and $\tau_{surface}$ are the minority carrier lifetimes related to recombination via the localized point defects as per the Shockley–Read–Hall (SRH) model and surface, respectively. The L_c value ($\approx L_{diff}$) of the n-type SnS single crystal (~ 200 nm) is much smaller than the L_c (~ 1 μm) value deemed sufficient for typical thin-film solar-cell materials.[19] Thus, J_{SC} (~ 20 mA cm^{-2}) may be increased further by reducing the concentration of defects that significantly affect τ_{SRH} and L_{diff}. For instance, optimizing the deposition conditions for Cu$_2$ZnSn(S,Se)$_2$ reduced the number of oxygen impurities, increased L_C from 300 to 900 nm, and significantly increased J_{SC} from 8.3 to 29.6 mA cm^{-2}.[29] In the case of the devices fabricated in the present study, when L_c was increased to 1000 nm, J_{SC} increased significantly to ~ 28 mA cm^{-2}, resulting in a PCE of 10% (Fig. 6 and Table II). Thus, reducing the dopant concentration of the SnS single crystal increases both V_{OC} (by reducing J_0) and J_{SC} (by enhancing L_C). Because the SnS single crystals were prepared using a simple flux method, the saturated Br concentration under growth temperature was incorporated into the single crystals, and it is difficult to decrease the Br concentration. Therefore, it is necessary to modify the condition of the flux method or use

other methods, such as the Bridgeman technique, to reduce the Br concentration in the SnS single crystals.

Although the FF value increased by enhancing the conductivity of the MoO$_3$ layer, the value was low (40%–50%). Even when J_0 and L_C were decreased and increased, respectively, FF was $\sim 60\%$ (Table II). To further increase FF, attempts should be made to reduce R_s and increase R_{sh}, as both affect FF.[28] R_s is relatively large (4.2 Ω cm^{-2}) and, thus, can be reduced. When R_s was reduced to 1 Ω cm^{-2} after decreasing J_0 and increasing L_C, FF improved from 59% to 69%, and PCE increased to 11.8% (Table II). By contrast, when R_{sh}, which is relatively large (~ 300 Ω cm^{-2}), was increased to 1000 Ω cm^{-2}, FF only improved from 59% to 61%. Therefore, it is better to improve FF by reducing R_s than by increasing R_{sh}.

The R_s values of ITO (300 nm), SnS (50 μm), and the highly conductive MoO$_3$ thin film (3 nm) were $\sim 5 \times 10^{-8}$, $\sim 5 \times 10^{-3}$, and $\sim 1 \times 10^{-2}$ Ω cm^{-2}, respectively, and they were significantly smaller than the R_s of the device. Therefore, R_S is mostly influenced by the resistance at the MoO$_3$/SnS, SnS/GaIn, and/or MoO$_3$/ITO interfaces. Thus, future studies should foremost evaluate the SnS/GaIn and MoO$_3$/ITO interfacial resistances and consider substituting ITO and GaIn with more suitable contact materials.

V. CONCLUSIONS

In this study, solar cells based on the interface between n-type single-crystalline SnS and MoO$_3$ thin films were fabricated, and their photovoltaic performances were evaluated. A PCE as high as 4.2% could be achieved. The optimal MoO$_3$ thickness was 3–6 nm, and enhancing the MoO$_3$ conductivity reduced R_s and slightly increased FF. The maximum V_{OC} was 437 mV, which is the highest ever for SnS solar cells. However, it was not as high as expected (700–800 mV). To increase V_{OC}, it is necessary to decrease J_0 by limiting interfacial recombination. This can be achieved by reducing the concentration of Br in the SnS single crystals. To date, a low V_{OC} has limited the PCE of SnS solar cells. This study demonstrates that it is possible to increase the V_{OC} of these cells. Specifically, it is possible to ensure a large light absorption coefficient and, hence, a high degree of light absorption even in the case of thin films by fabricating a junction between n-type SnS[30] and MoO$_3$ thin films.

SUPPLEMENTARY MATERIAL

See the supplementary material for Figs. S1–S4 and Table S1. Figure S1 shows the XPS spectra of the high- and low-conductivity

MoO$_3$ thin films. Figure S2 and Table S1 show the photovoltaic performance of the devices based on the MoO$_3$ thin films with thicknesses of 1–12 nm. Figure S3 shows the bandgap of the absorber layer as determined by EQE. Figure S4 shows the EQE spectra of the various fabricated solar cells.

AUTHOR DECLARATIONS

Conflict of Interest

The authors have no conflicts to disclose.

Author Contributions

Issei Suzuki: Conceptualization (lead); Data curation (lead); Funding acquisition (equal); Investigation (lead); Visualization (lead); Writing – original draft (lead). **Zexin Lin**: Data curation (lead); Investigation (lead). **Taichi Nogami**: Investigation (supporting); Writing – review & editing (supporting). **Sakiko Kawanishi**: Resources (lead); Writing – review & editing (supporting). **Binxiang Huang**: Investigation (supporting); Writing – review & editing (supporting). **Andreas Klein**: Funding acquisition (equal); Supervision (equal); Writing – review & editing (supporting). **Takahisa Omata**: Supervision (equal); Writing – review & editing (lead).

DATA AVAILABILITY

The data that support the findings of this study are available from the corresponding author upon reasonable request.

REFERENCES

[1] A. Zakutayev, J. D. Major, X. Hao, A. Walsh, J. Tang, T. K. Todorov, L. H. Wong, and E. Saucedo, J. Phys. Energy **3**, 032003 (2021).

[2] T. H. Nguyen, T. Kawaguchi, J. Chantana, T. Minemoto, T. Harada, S. Nakanishi, and S. Ikeda, ACS Appl. Mater. Interfaces **10**, 5455 (2018).

[3] A. Kanai and M. Sugiyama, Sol. Energy Mater. Sol. Cells **231**, 111315 (2021).

[4] Y. C. Choi, D. U. Lee, J. H. Noh, E. K. Kim, and S. I. Seok, Adv. Funct. Mater. **24**, 3587 (2014).

[5] S. Kawanishi, I. Suzuki, S. R. Bauers, A. Zakutayev, H. Shibata, H. Yanagi, and T. Omata, Sol. RRL **5**, 2000708 (2021).

[6] D. G. Moon, S. Rehan, D. H. Yeon, S. M. Lee, S. J. Park, S. Ahn, and Y. S. Cho, Sol. Energy Mater. Sol. Cells **200**, 109963 (2019).

[7] T. D. Nguyen, V. T. Dang, N. M. Hung, V. K. Arepalli, J. Kim, M. Raj, and T. T. O. Nguyen, Surf. Interfaces **25**, 101151 (2021).

[8] I. Suzuki, S. Kawanishi, T. Omata, and H. Yanagi, J. Phys. Energy **4**, 042002 (2022).

[9] H. S. Yun, B. w. Park, Y. C. Choi, J. Im, T. J. Shin, and S. I. Seok, Adv. Energy Mater. **9**, 1901343 (2019).

[10] I. Suzuki, B. Huang, S. Kawanishi, T. Omata, and A. Klein, J. Phys. Chem. C **126**, 020570 (2022).

[11] A. Klein and W. Jaegermann, Appl. Phys. Lett. **74**, 2283 (1999).

[12] A. Yamada, K. Matsubara, K. Sakurai, S. Ishizuka, H. T. Hajime, S. Tomoyuki Baba, Y. Kimura, S. Nakamura, H. Nakanishi, and S. Niki, MRS Online Proc. Libr. **865**, 519 (2005).

[13] S. Kawanishi, I. Suzuki, T. Ohsawa, N. Ohashi, H. Shibata, and T. Omata, Cryst. Growth Des. **20**, 5931 (2020).

[14] S. Yazdani, R. Kashfi-Sadabad, T. D. Huan, M. D. Morales-Acosta, and M. T. Pettes, Langmuir **34**, 6296 (2018).

[15] S.-Y. Lin, Y.-C. Chen, C.-M. Wang, P.-T. Hsieh, and S.-C. Shih, Appl. Surf. Sci. **255**, 3868 (2009).

[16] M. T. Greiner, L. Chai, M. G. Helander, W.-M. Tang, and Z.-H. Lu, Adv. Funct. Mater. **22**, 4557 (2012).

[17] S. S. Hegedus and W. N. Shafarman, Prog. Photovoltaics **12**, 155 (2004).

[18] *Spectroscopic Ellipsometry for Photovoltaics: Volume 2: Applications and Optical Data of Solar Cell Materials*, edited by H. Fujiwara and R. W. Collins (Springer International Publishing, Cham, 2018).

[19] A. Nakane, H. Tampo, M. Tamakoshi, S. Fujimoto, K. M. Kim, S. Kim, H. Shibata, S. Niki, and H. Fujiwara, J. Appl. Phys. **120**, 064505 (2016).

[20] H. Fujiwara and M. Kondo, Phys. Rev. B **71**, 075109 (2005).

[21] P. Sinsermsuksakul, J. Heo, W. Noh, A. S. Hock, and R. G. Gordon, Adv. Energy Mater. **1**, 1116 (2011).

[22] R. E. Banai, H. Lee, M. A. Motyka, R. Chandrasekharan, N. J. Podraza, J. R. S. Brownson, and M. W. Hom, IEEE J. Photovoltaics **3**, 1084 (2013).

[23] D. Chua, S. B. Kim, P. Sinsermsuksakul, and R. Gordon, Appl. Phys. Lett. **114**, 213901 (2019).

[24] P. S. Pawar, J. Y. Cho, K. E. Neerugatti, S. Sinha, T. R. Rana, S. Ahn, and J. Heo, ACS Appl. Mater. Interfaces **12**, 7001 (2020).

[25] H. H. Park, R. Heasley, L. Sun, V. Steinmann, R. Jaramillo, K. Hartman, R. Chakraborty, P. Sinsermsuksakul, D. Chua, T. Buonassisi, and R. G. Gordon, Prog. Photovoltaics **23**, 901 (2015).

[26] W. Wang, M. T. Winkler, O. Gunawan, T. Gokmen, T. K. Todorov, Y. Zhu, and D. B. Mitzi, Adv. Energy Mater. **4**, 1301465 (2014).

[27] M. P. Suryawanshi, S. W. Shin, U. V. Ghorpade, K. V. Gurav, C. W. Hong, G. L. Agawane, S. A. Vanalakar, J. H. Moon, J. H. Yun, P. S. Patil, J. H. Kim, and A. V. Moholkar, Electrochim. Acta **150**, 136 (2014).

[28] J. Nelson, *The Physics of Solar Cells* (Imperial College Press, 2003).

[29] Y. Zhang, N. Suyama, M. Goto, M. Yin, and A. Yamada, Appl. Phys. Express **6**, 072302 (2013).

[30] I. Suzuki, S. Kawanishi, S. R. Bauers, A. Zakutayev, Z. Lin, S. Tsukuda, H. Shibata, M. Kim, H. Yanagi, and T. Omata, Phys. Rev. Mater. **5**, 125405 (2021).